

Supporting Information

Low-valent cobalt oxide co-catalyst boosting photocatalytic water oxidation via enhanced hole-capturing ability

Shi Yang Xiao^a, Yuanwei Liu^a, Xue Feng Wu^a, Li Ting Gan^a, Hao Yang Lin^a, Li Rong
Zheng^b, Sheng Dai^c, Peng Fei Liu^{a*}, Hua Gui Yang^{a*}

^a Key Laboratory for Ultrafine Materials of Ministry of Education, Shanghai Engineering Research Center of Hierarchical Nanomaterials, School of Materials Science and Engineering, East China University of Science and Technology, 130 Meilong Road, Shanghai 200237, China.

^b Beijing Synchrotron Radiation Facility, Institute of High Energy Physics, Chinese Academy of Sciences, Beijing 100049, China.

^c Key Laboratory for Advanced Materials and Feringa Nobel Prize Scientist Joint Research Center, Institute of Fine Chemicals, School of Chemistry and Molecular Engineering, East China University of Science and Technology, 130 Meilong Road, Shanghai 200237, China.

Emails: hgyang@ecust.edu.cn; pfliu@ecust.edu.cn

Experimental section

Chemical and reagents

For the preparation of cobalt-decorated TaON, Ta₂O₅ (Aladdin Chemicals, 99%), ethanol (General Reagent Chemicals, 99.7%), cobalt (II) acetylacetonate (Acros Organics Chemicals, 99%) and cobalt (III) acetylacetonate (Alfa Aesar, 99%) were used. Silver nitrate (AgNO₃, Damas-Beta Chemicals, 99%), ferric nitrate nonahydrate (Fe(NO₃)₃·9H₂O, Sinopharm Chemicals, 99 %) and sodium thiosulfate (Na₂S₂O₈, Aladdin Chemicals, 99%) were employed as a sacrificial electron donor, and lanthanum oxide (La₂O₃, Sinopharm Chemicals, 99.99%) was applied as a buffer agent. All chemicals were used as-purchased without further purification.

Synthesis of photocatalysts

TaON was synthesized from commercially available Ta₂O₅ by a thermal nitridation process. Cobalt (II) acetylacetonate (Co(acac)₂) and cobalt (III) acetylacetonate (Co(acac)₃) were chosen as the raw materials. CoO_x co-catalysts with different oxidation states were loaded on TaON by the photochemical metal-organic deposition method under the vacuum condition. For a specific synthesis, 100 mg of TaON nanoparticles and 10 mL Co(acac)₂ or Co(acac)₃ ethanol solution with different concentrations (0.25, 0.50, 1.50 and 2.50 mg·mL⁻¹) were mixed into 30 mL distilled water. With Co(acac)₂ as the precursor, the as prepared samples with different concentrations were labeled as TaON/LVCoO_x-2.5, TaON/LVCoO_x-5, TaON/LVCoO_x-15 and TaON/LVCoO_x-25, while the samples using Co(acac)₃ as precursors with different concentrations were labeled as TaON/HVCoO_x-2.5, TaON/HVCoO_x-5, TaON/HVCoO_x-15 and TaON/HVCoO_x-25. Samples of TaON/LVCoO_x-5 and TaON/HVCoO_x-5 are further abbreviated as TaON/LVCoO_x and TaON/HVCoO_x, respectively. In order to exclude the impact of dissolved oxygen on the valence state, the precursor solution was evacuated by vacuum pump, and then the system was irradiated under 300 W Xenon lamp for different time (15 min, 30 min, 1 h and 3 h). Finally, the prepared powder was collected by centrifugation, washed with

distilled water and ethanol respectively for three times and then dried at 333 K for over 12 h in a vacuum oven to obtain the purged products.

Post oxidation or nitridation treatment on the TaON/LVCoO_x samples were also carried out. Oxidation treatment was carried out by calcining the samples in the muffle furnace under the air environment at 573 K for 1 h, while nitridation treatment was carried out by calcining the powder in the tube furnace with the flow of NH₃ (50 sccm) at 773 K for 1 h.

Characterization

X-ray diffraction patterns (XRD, D/MAX 2550 VB/PC) were acquired to study the crystal structure. The composition of surface elements and corresponding valence state were determined by X-ray photoelectron measurements (XPS, ESCALAB 250Xi), and normalized to the C 1s peak (284.6 eV) for each sample. The morphologies and particle size of as-prepared samples were examined by scanning electron microscopy (SEM, HITACHI S4800), high-resolution transmission electron microscopy (HRTEM, JEM 2100, 200 kV) and high-angle annular dark-field scanning transmission electron microscopy (HAADF-STEM, ThermoFisher Talos F200X). Energy dispersive X-ray spectroscopy (EDS) was carried out using 4 in-column Super-X detectors. Fourier transform infrared (FTIR) spectroscopy was carried out using a Jasco FTIR-4100 (Japan) spectrometer. The optical absorption of samples was analyzed by Ultraviolet-visible (UV-vis) diffuse reflection spectra using a UV-vis spectrophotometer (CARY500). Photoluminescence spectra (PL) were conducted under 420 nm by an Edinburgh Instruments (FLSP 920) system. The contents of element Co in varied samples were measured by inductively coupled plasma-atomic emission spectroscopy (ICP-AES, Varian 710ES). With Co foil, CoO and Co₃O₄ were used as the reference samples, Co K-edge X-ray absorption fine structure analysis was performed on the 1W1B beamline of the Beijing Synchrotron Radiation Facility, China, operated at ~200 mA and ~2.5 GeV.

Photocatalytic activity test

The solar-driven water oxidation reactions were carried out in a glass gas-closed

circulation system (CEL-SPH2N, CEAULight, China) with a top irradiation-type reaction vessel. 25 mg of the as-prepared powders were well-dispersed in 50 mL aqueous solution with constant stirring containing 150 mg AgNO₃ as the sacrificial reagent for photocatalytic water oxidation. 50 mg La₂O₃ was added to adjust the pH value of solution, which was measured at ca. 8.5. Photocatalytic performances with Na₂S₂O₈ and Fe(NO₃)₃ as electron scavengers were also conducted. The mixture was put into ultrasonic bath for 10 min and then evacuated by vacuum pump to ensure the vacuum condition before the test. 300 W Xenon lamp (CEL-HXF300) equipped with an ultraviolet cut-off filter (> 420 nm) was used to irradiate from the top side with a flow of cooling water maintaining the reaction system at room temperature. Since deposition of Ag nanoparticles often decreases the O₂ evolution rate, the photocatalytic oxygen evolution activity was estimated from the initial gas evolution rate (the O₂ evolution rate in the initial 1 h irradiation).

The apparent quantum efficiency (AQE) was conducted using the same experimental setup, except that different cut-off filters were employed to obtain monochromatic light with specific wavelengths ($\lambda = 380, 420, 475, 520, 550$ and 630 nm). 25 mg of photocatalyst was dispersed in aqueous solution (50 mL) containing 150 mg of AgNO₃ and 50 mg of La₂O₃. AQE for O₂ production at monochromatic light irradiation was estimated as following:

$$AQE(\%) = \frac{4 \times \text{Number of evolved } O_2 \text{ molecules}}{\text{Number of incident photons}} \times 100\%$$

$$= \frac{4 \times C \times N_A}{S \times P \times t \times \frac{\lambda}{h \times c}} \times 100\%$$

Photoelectrochemical measurements

Tantalum-based photoelectrodes were fabricated by using the electrophoretic deposition (EPD) method to study its photo-electrochemical properties. Suspension for electrophoretic deposition was obtained by dispersing 20 mg of iodine and 30 mg of catalysts in 30 mL of acetone under sonication. Two parallel conducting fluorine doped tin oxide (FTO) glass with a dimension of 2×1 cm² were immersed into the mixed solution with a distance of 1 cm between them. A stable 10 V voltage was applied for

3 min using a potentiostatic control during the electrophoretic deposition process. The electrodes were dried naturally and then a few drops of diluted tantalum chloride (TaCl_5) methanol solution (10 mM) were coated on the surface of the electrodes. Finally, the electrodes were heated in a flow of ammonia (20 sccm) at 673 K for 30 min and cooled naturally to room temperature.

The electrochemical impedance spectroscopy (EIS) was performed with an electrochemical analyzer in a three-electrode system, in which the Ag/AgCl/KCl (3.5 M) electrode works as a reference electrode and Pt foil works as a counter electrode. 0.5 M Na_2SO_4 aqueous solution is considered as the electrolyte. Impedance analysis was carried out by applying an AC signal from 10^5 to 10^{-1} Hz with 10 mV amplitude under open-circuit voltage. Transient photocurrent response measurements were performed under irradiation condition using a solar light simulator (Oriel, 91160, AM 1.5 globe) with light intensity of 100 mW cm^{-2} at a bias potential of 1.23 V vs. reversible hydrogen electrode (RHE). The transient open-circuit voltage decay (OCVD) measurements were taken for 400 seconds (s) in all, and the light on and off were controlled at 40 and 100 s from the start, respectively.

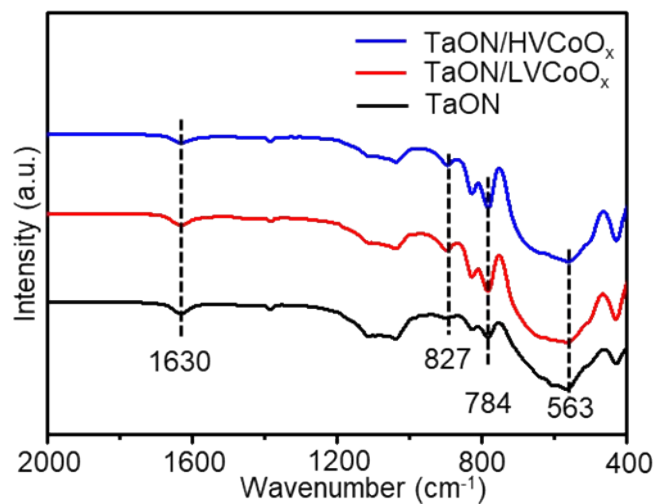


Fig. S1 FTIR spectra of the as-prepared TaON, TaON/LVCoO_x and TaON/HVCoO_x samples, exhibiting negligible difference, which demonstrates that no obvious organic ligands were left on the TaON surface. Notes: The peaks at 784 and 563 cm⁻¹ are the characteristic absorption band of Ta-N bonds; the peak at 827 cm⁻¹ is related to Ta-O-Ta or Ta-O stretching vibration modes of TaON; the peak around 1626 cm⁻¹ corresponds to the N-H bending vibrations^{1,2}.

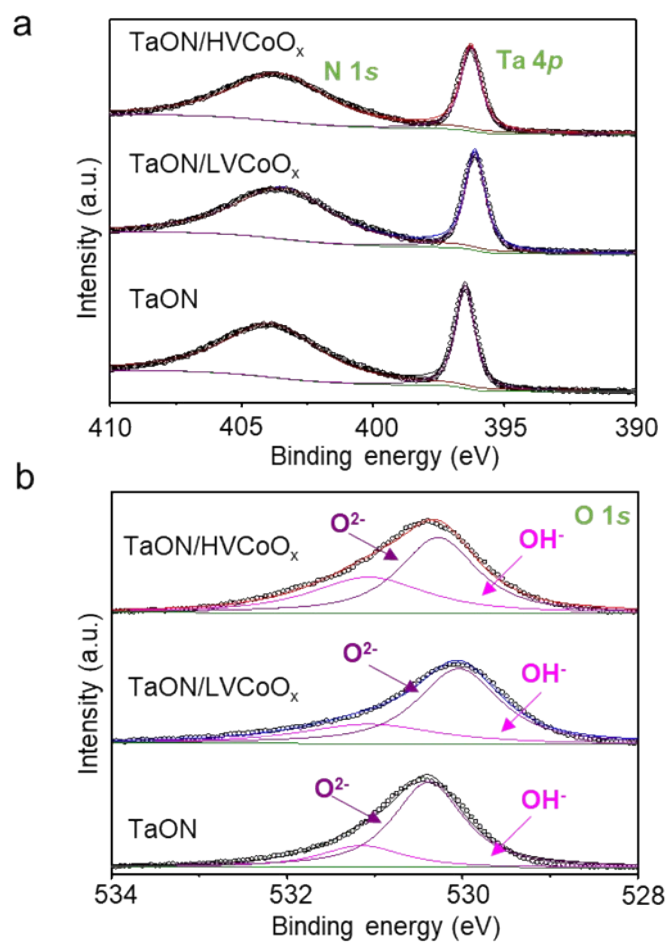


Fig. S2 XPS spectra of TaON/LVCoO_x, TaON/HVCoO_x and TaON samples in the (a) Ta 4p, N 1s (b) O 1s regions, suggesting the strong electronic interaction between the CoO_x co-catalysts and TaON, which results in the shift of the peaks to the lower binding energy.

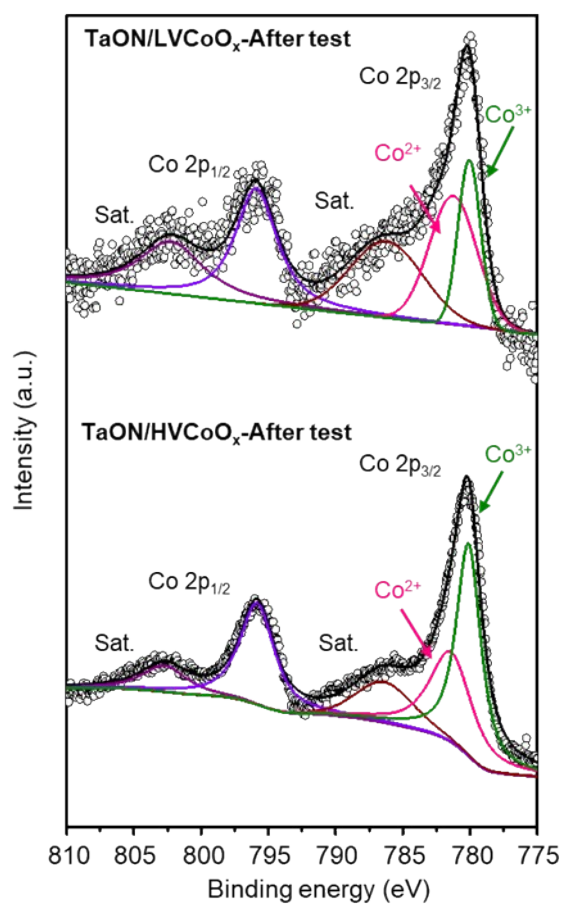


Fig. S3 XPS spectra of TaON/LVCoO_x and TaON/HVCoO_x in the Co 2p region after photocatalytic tests for 2 h with Na₂S₂O₈ as the sacrificial agent, indicating the change of oxidation state of cobalt after photocatalytic tests.

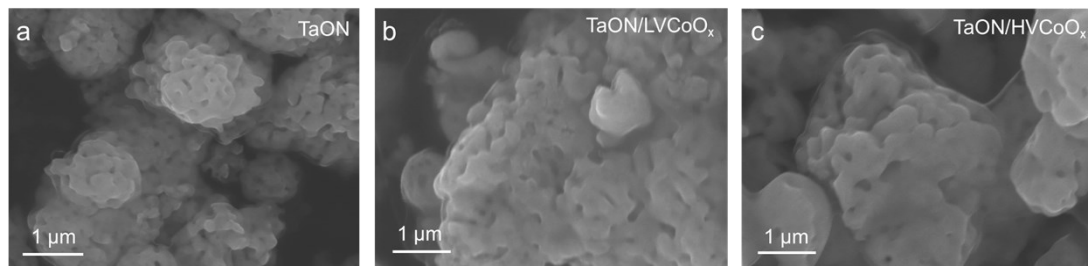


Fig. S4 SEM images of samples (a) TaON, (b) TaON/LVCoO_x and (c) TaON/HVCoO_x, indicating the similar morphology before and after photodeposition process.

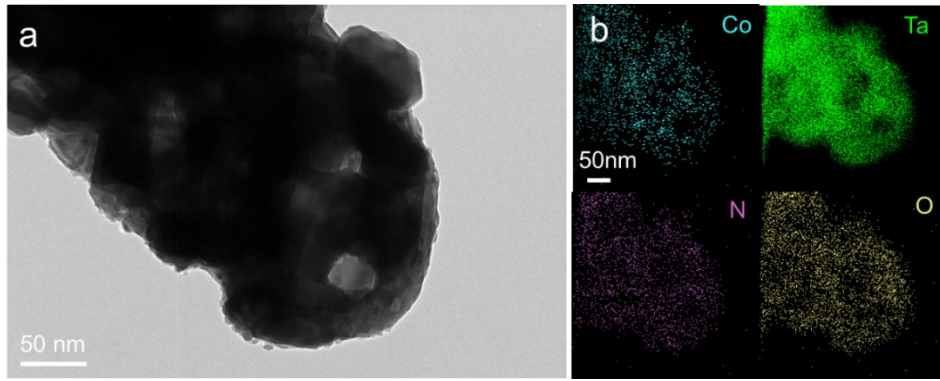


Fig. S5 (a) The TEM image of TaON/LVCoO_x and (b) corresponding elemental mapping images for Co, Ta, N and O elements.

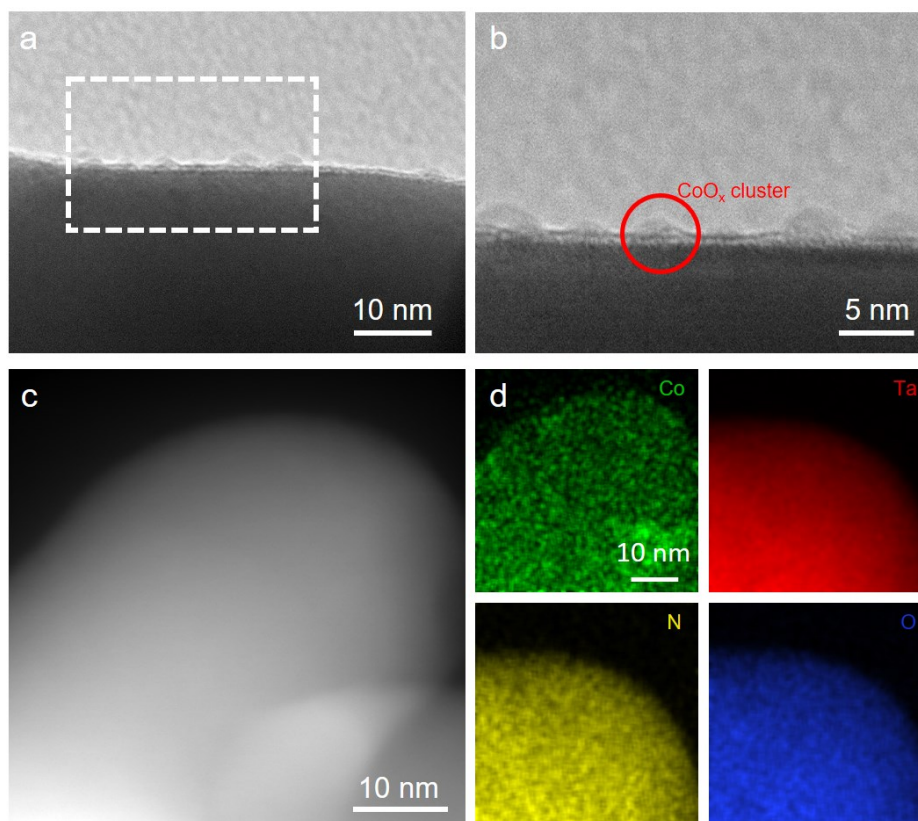


Fig. S6 (a, b) TEM images of TaON/HVCoO_x samples, indicating similar morphologies of CoO_x co-catalysts as the TaON/HVCoO_x sample, which also suggests the amorphous feature. (c) The STEM image of TaON/HVCoO_x and (d) corresponding elemental mapping images for Co, Ta, N and O elements, exhibiting the uniform distribution of CoO_x co-catalyst.

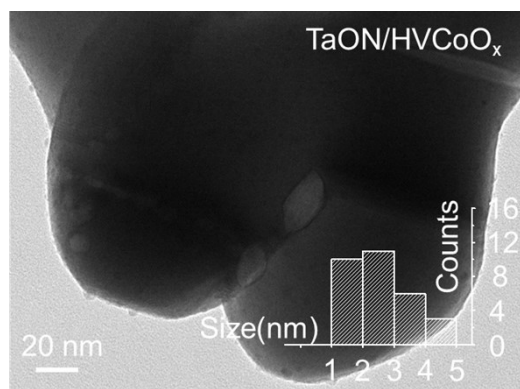


Fig. S7 Typical TEM image of TaON/HVCoO_x samples. Inset: the particle size distribution of CoO_x, indicating that particle size as estimated from TEM image is around 2.6 nm.

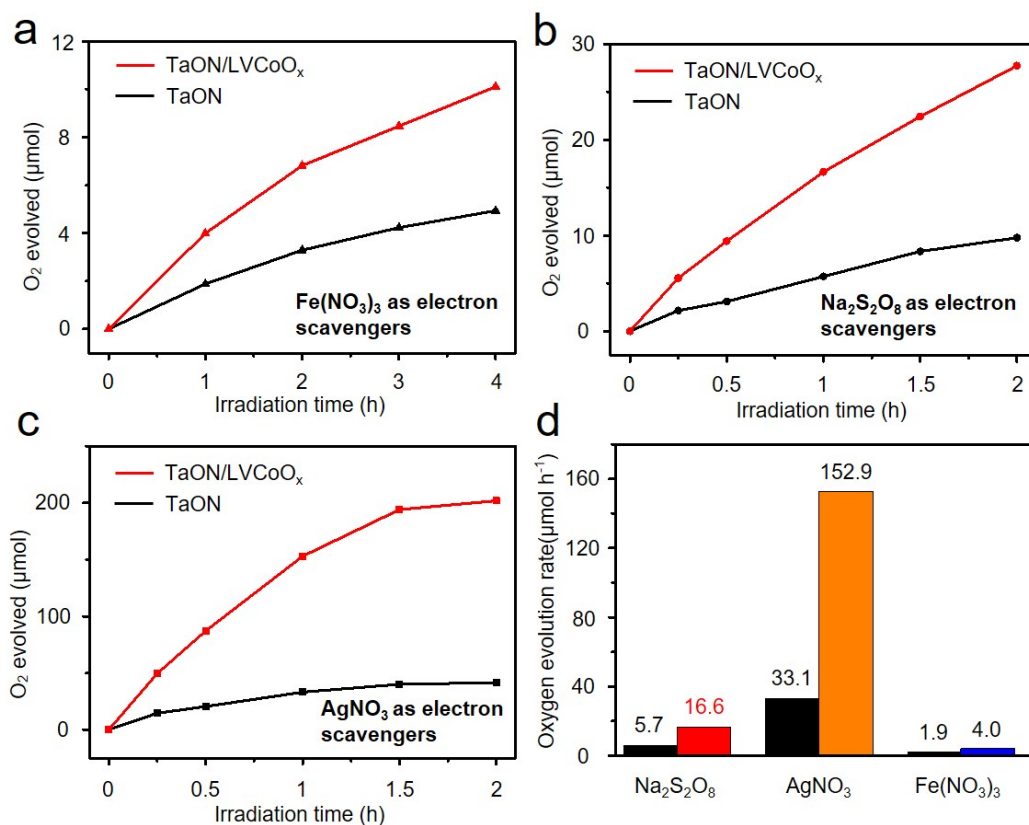


Fig. S8 Time courses of O₂ evolution on the TaON/LVCoO_x and TaON with (a) Fe(NO₃)₃·9H₂O, (b) Na₂S₂O₈ and (c) AgNO₃ as sacrificial agents respectively. Test conditions: (a) 100 mg catalyst, 350 mg Fe(NO₃)₃·9H₂O, 50 mL H₂O, 300 W Xenon lamp ($\lambda > 420$ nm); (b) 25 mg catalyst, 210 mg Na₂S₂O₈, pH adjusted to 13 by NaOH, 50 mL H₂O, 300 W Xenon lamp ($\lambda > 420$ nm); (c) 25 mg catalyst, 150 mg AgNO₃, 50 mg La₂O₃ (as a buffer agent to maintain the pH value of the reaction solution to be ~8.5), 50 mL H₂O, 300 W Xenon lamp ($\lambda > 420$ nm); (d) Comparison of oxygen evolution rate with Fe(NO₃)₃·9H₂O, Na₂S₂O₈, and AgNO₃ as sacrificial agents, respectively.

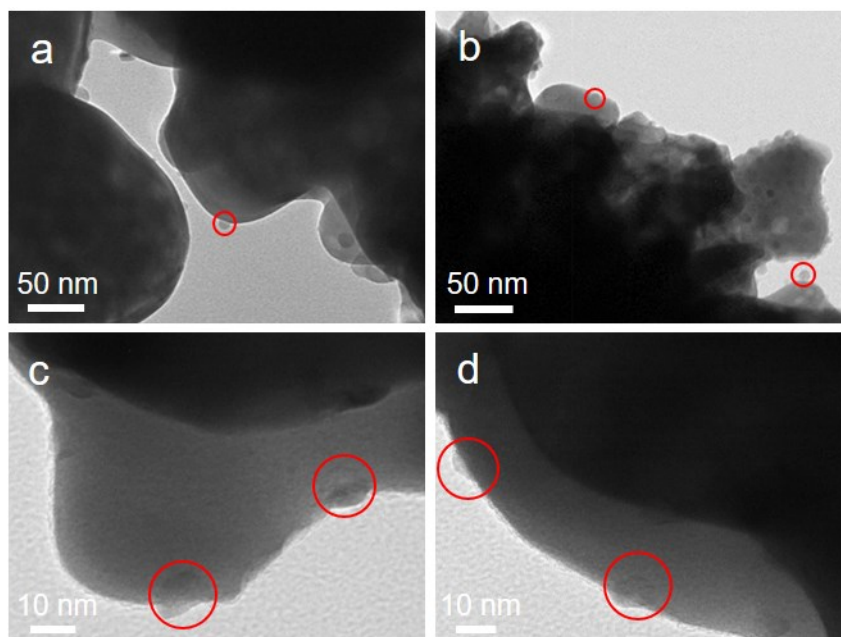


Fig. S9 (a, b) TEM images of TaON/LVCoO_x-N. (c, d) TEM images of TaON/LVCoO_x-O. The TEM images of the samples obtained from post oxidation or nitridation treatment indicate that the CoO_x co-catalysts are aggregated to an enlarged particle size.

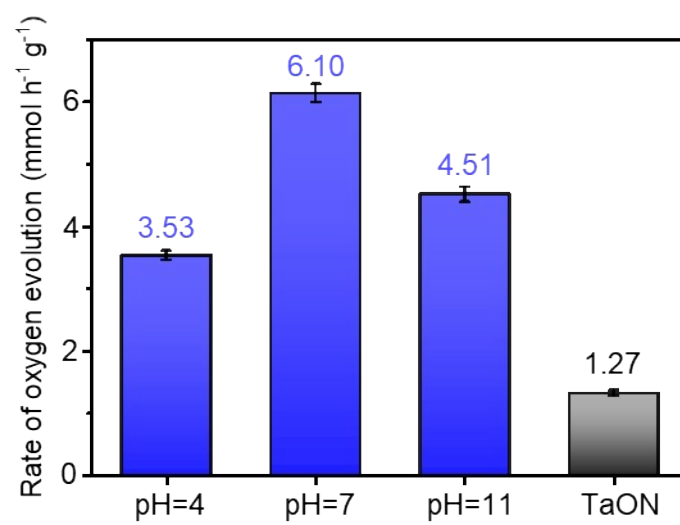


Fig. S10 Photocatalytic water oxidation activities of TaON/LVCoO_x which were obtained under different pH, indicating that the neutral deposition solution is beneficial for the OER activity.

Table S1. The CoO_x contents in the samples with different precursor mass and photodeposition time.

Precursor mass	Photodeposition time	Co wt% (ICP-AES data)
Co(acac) ₂ -5 mg	0.5 h	0.15
Co(acac) ₂ -5 mg	3 h	0.26
Co(acac) ₂ -35 mg	0.5 h	0.28
Co(acac) ₃ -5 mg	0.5 h	0.12
Co(acac) ₃ -5 mg	3 h	0.19
Co(acac) ₃ -35 mg	0.5 h	0.18

Table S2. CoO_x contents in the samples with different amounts of inorganic or organic cobalt precursors.

Precursor	Precursor mass	Co wt% (ICP-AES data)
Co(acac) ₂	5 mg	0.15
Co(acac) ₂	35 mg	0.28
Co(acac) ₃	5 mg	0.12
Co(acac) ₃	35 mg	0.18
CoCl ₂	5 mg	0.05
CoCl ₂	35 mg	0.06
Co(NO ₃) ₂	5 mg	0.09
Co(NO ₃) ₂	35 mg	0.11

Notes: The photodeposition time of different samples for ICP characterizations is 0.5 h.

Table S3. Photocatalytic performance comparison of tantalum (titanium) -based photocatalysts.

Materials	AQY (%)	Activity ($\lambda > 420$ nm) ($\mu\text{mol h}^{-1} \text{g}^{-1}$)	References
TaON/LVCoO_x	21.2% (420 nm)	6120 ± 170	This work
Ta ₃ N ₅ @NaTaON core-shell nanocube	16.8% (420 nm)	10920	<i>Adv. Energy Mater.</i> 2017, 7 , 1700171 ³
MgO-modified Ta ₃ N ₅ -CoO _x	11.3% (500-600 nm)	6000	<i>Angew. Chem. Int. Ed.</i> 2015, 54 , 3047-3051 ⁴
Na ₂ CO ₃ /Ta ₃ N ₅ - CoO _x	5.2% (500-600 nm)	4550	<i>J. Am. Chem. Soc.</i> 2012, 134 , 19993-19996 ⁵
Ta ₃ N ₅ -CoO _x	19.4% (440 nm)	4500	<i>Chem. Mater.</i> 2015, 27 , 5685-5694 ⁶
core/shell Ta ₃ N ₅ - CoO _x	/	3920	<i>Angew. Chem. Int. Ed.</i> 2013, 52 , 11252- 11256 ⁷
LaTiO ₂ N-CoO _x	27.1% (440 nm)	3680	<i>J. Am. Chem. Soc.</i> 2012, 134 , 8348-8351 ⁸
Ta ₃ N ₅ -CoO _x -Rh	28% (500 nm)	2660	<i>ACS Catal.</i> 2016, 6 , 4117-4126 ⁹
LaTiO ₂ N	/	2600	<i>J. Phys. Chem. C</i> 2013, 118 , 16344-16351 ¹⁰
Zr-Ta ₃ N ₅	/	2490	<i>ACS Appl. Mater. Interfaces</i> 2016, 8 , 35407- 35418 ¹¹
Ta ₃ N ₅ /La ₂ O ₃	10% (420-600 nm)	2100	<i>Chem. Lett.</i> 2002, 31 , 736-737 ¹²
Ta ₃ N ₅	/	2050	<i>Mater. Res. Bull.</i> 2012, 47 , 3605-3611 ¹³
TaON	34% (420-600 nm)	1650	<i>Chem. Commun.</i> 2002, DOI: 10.1039/b202393h, 1698-1699 ¹⁴
LaTiO ₂ N	/	1650	<i>Nano Lett.</i> 2014, 14 , 1038-1041 ¹⁵
Zn-TPP dimer/TaON	/	1385	<i>Catalysts</i> 2013, 3 , 614-624 ¹⁶
Ta ₃ N ₅ QDs/TaON	67% (420 nm)	1041	<i>J. Mater. Chem.</i> 2012, 22 , 21972-21978 ¹⁷
Ta ₃ N ₅	/	400	J. Fu, S. E. Skrabalak, <i>J. Mater. Chem. A</i> 2016, 4 , 8451-8457 ¹⁸
LnTaO ₂ N	/	380	<i>Phys. Chem. Chem. Phys.</i> 2017, 19 , 22210- 22220 ¹⁹
BaTaO ₂ N	/	220	<i>Angew. Chem. Int. Ed.</i> 2013, 52 , 6488- 6491 ²⁰
Na _{0.25} La _{0.75} TaO _{1.5} N ₁	/	50	<i>J. Mater. Chem. A</i> 2013, 1 , 3667-3674 ²¹

Notes: The activities mentioned above were all calculated based on the oxygen evolution amount of the 1st hour's test.

References

- [1] H. Jiang, W. Zhang, S. Zang, W. Zhang, *Int. J. Hydrogen Energy* 2019, **44**, 24218-24227.
- [2] R. Nakamura, T. Tanaka, Y. Nakato, *J. Phys. Chem. B* 2005, **109**, 8920-8927.
- [3] J. Hou, Y. Wu, S. Cao, F. Liang, Z. Lin, Z. Gao, L. Sun, *Adv. Energy Mater.* 2017, **7**, 1700171.
- [4] S. Chen, S. Shen, G. Liu, Y. Qi, F. Zhang, C. Li, *Angew. Chem. Int. Ed.* 2015, **54**, 3047-3051.
- [5] S. S. Ma, T. Hisatomi, K. Maeda, Y. Moriya, K. Domen, *J. Am. Chem. Soc.* 2012, **134**, 19993-19996.
- [6] E. Nurlaela, S. Ould-Chikh, I. Llorens, J. -L. Hazemann, K. Takanabe, *Chem. Mater.* 2015, **27**, 5685-5694.
- [7] D. Wang, T. Hisatomi, T. Takata, C. Pan, M. Katayama, J. Kubota, K. Domen, *Angew. Chem. Int. Ed.* 2013, **52**, 11252-11256.
- [8] F. Zhang, A. Yamakata, K. Maeda, Y. Moriya, T. Takata, J. Kubota, K. Teshima, S. Oishi, K. Domen, *J. Am. Chem. Soc.* 2012, **134**, 8348-8351.
- [9] E. Nurlaela, H. Wang, T. Shinagawa, S. Flanagan, S. Ould-Chikh, M. Qureshi, Z. Mics, P. Sautet, T. Le Bahers, E. Cánovas, M. Bonn, K. Takanabe, *ACS Catal.* 2016, **6**, 4117-4126.
- [10] A. E. Maegli, S. Pokrant, T. Hisatomi, M. Trottmann, K. Domen, A. Weidenkaff, *J. Phys. Chem. C* 2013, **118**, 16344-16351.
- [11] Y. Wang, D. Zhu, X. Xu, *ACS Appl. Mater. Interfaces* 2016, **8**, 35407-35418.
- [12] G. Hitoki, A. Ishikawa, T. Takata, J. N. Kondo, M. Hara, K. Domen, *Chem. Lett.* 2002, **31**, 736-737.
- [13] Z. Wang, J. Wang, J. Hou, K. Huang, S. Jiao, H. Zhu, *Mater. Res. Bull.* 2012, **47**, 3605-3611.
- [14] G. Hitoki, T. Takata, J. N. Kondo, M. Hara, H. Kobayashi, K. Domen, *Chem. Commun.* 2002, DOI: 10.1039/b202393h, 1698-1699.
- [15] M. Matsukawa, R. Ishikawa, T. Hisatomi, Y. Moriya, N. Shibata, J. Kubota, Y. Ikuhara, K. Domen, *Nano Lett.* 2014, **14**, 1038-1041.

- [16] H. Hagiwara, M. Nagatomo, C. Seto, S. Ida, T. Ishihara, *Catalysts* 2013, **3**, 614-624.
- [17] Z. Wang, J. Hou, S. Jiao, K. Huang, H. Zhu, *J. Mater. Chem.* 2012, **22**, 21972-21978.
- [18] J. Fu, S. E. Skrabalak, *J. Mater. Chem. A* 2016, **4**, 8451-8457.
- [19] M. Hojamberdiev, M. F. Bekheet, J. N. Hart, J. J. M. Vequizo, A. Yamakata, K. Yubuta, A. Gurlo, M. Hasegawa, K. Domen, K. Teshima, *Phys. Chem. Chem. Phys.* 2017, **19**, 22210-22220.
- [20] K. Maeda, D. Lu, K. Domen, *Angew. Chem. Int. Ed.* 2013, **52**, 6488-6491.
- [21] K. Ueda, H. Kato, M. Kobayashi, M. Hara, M. Kakihana, *J. Mater. Chem. A* 2013, **1**, 3667-3674.